MRL 87-64(TR)c.2
I-M993417c.2 CPUB

Energy, Mines and Resources Canada | Energie, Mines et Ressources Canada

CANMET

Canada Centre for Mineral and Energy Technology | Centre canadien de la technologie des minéraux et de l'énergie

CHARACTERIZATION OF LONG-LIVED RADIOACTIVE DUST EMISSIONS IN PHYSICO-CHEMICAL OPERATIONS IN A URANIUM MILL

J. BIGU AND E. EDWARDSON

ELLIOT LAKE LABORATORY

OCTOBER 1986

MINING RESEARCH LABORATORIES
DIVISION REPORT MRL 87-64 (TR)

c.2 CPUB

MRL 87-64(TR)c.2

Canmet Information Centre
Centre d'information de Canmet
JAN 24 1977
555, rue Booth St.
Ottawa, Ontario K1A 0G1

1-7993417c.2
CPUB

CHARACTERIZATION OF LONG-LIVED RADIOACTIVE DUST EMISSIONS IN PHYSICO-CHEMICAL OPERATIONS IN A URANIUM MILL

by

J. Bigu* and E. Edwardson**

ABSTRACT

The characteristics of long-lived radioactive dust clouds generated in several physico-chemical operations in a uranium mill have been investigated. The study consisted of the determination of dust size distribution, and of the size distribution of radionuclides associated with particulate matter in the size range <0.1 to 26 μm. Experiments were conducted using several cascade impactors operating at different sampling flow rates. Two different types of cascade impactors were used. Radionuclide identification was done using α-spectrometry and γ-spectrometry. Long-lived and short-lived radionuclides were identified in dust samples. The characteristics of the dust clouds depended on the physico-chemical operation. The following operations were studied: acid leaching, counter-current decantation, solvent extraction, yellowcake precipitation and drying. For the sake of completeness, yellowcake packaging is also included. In addition, other dust and radioactivity measurements have been carried out.

Keywords: Long-lived radioactive dust; Uranium; Mine mill.

*Research Scientist and Radiation/Respirable dust/Ventilation Project Leader,
**Technologist, CANMET, Energy, Mines and Resources Canada, Elliot Lake, Ontario.

CANMET LIBRARY
3 2329 00056888 6
c.2
CPUB

CARACTÉRISATION DES ÉMISSIONS DE POUSSIÈRES RADIOACTIVES À LONGUE PÉRIODE AU COURS DES OPÉRATIONS PHYSICO-CHIMIQUES D'UN BROYEUR D'URANIUM

par

J. Bigu* et E. Edwardson**

RÉSUMÉ

Les auteurs ont étudié les caractéristiques des nuages de poussière radioactive à longue période produits au cours des nombreuses opérations physico-chimiques d'un broyeur d'uranium. L'étude avait pour objet de déterminer la distribution granulométrique de la poussière et la distribution granulométrique des radionucléides associées à la matière subdivisée dans la plage des particules de <0,1 à 26 µm. On a fait des essais avec deux genres différents d'impacteurs à cascade fonctionnant à différentes vitesses d'écoulement échantillonnées. Deux différents genres d'impacteurs à cascade ont été utilisés. L'identification des radionucléides a été réalisée par spectrométrie α et par spectrométrie γ. Des radionucléides à longue période et à courte période ont été identifiées dans les échantillons de poussière. Les caractéristiques des nuages de poussières dépendent de l'opération physico-chimique. On a donc étudié les opérations suivantes: la lixiviation acide, la décantation à contre-courant, l'extraction par solvant, la précipitation et le séchage du concentré d'uranium y compris son emballage afin de compléter l'étude. Enfin, d'autres mesures de poussières et de rayonnement ont été effectuées.

Mots-clés: Poussières radioactives à longue période; Uranium; Broyeur de mine.

*Chercheur scientifique et Chef de projet Rayonnement/Poussières respirables/Ventilation;

**Technologiste, CANMET, Énergie, Mines et Ressources Canada, Elliot Lake, Ontario.

INTRODUCTION

Inhalation of airborne radionuclides poses a potential health hazard to occupational workers in the nuclear industry. For this reason, monitoring of radioactivity concentration levels for dose exposure calculation purposes is a subject of considerable practical interest.

Some concern has recently been expressed with regards to the inhalation of respirable dust (1-10 μm size range) containing long-lived radioisotopes, as once inhaled and lodged in the respiratory system they will remain active as long as they are not eliminated by natural biological processes.

There is sparse information available regarding the long-term health effects of worker's exposure to long-lived radioactive dust (LLRD) such as that produced in underground uranium mine and uranium mill operations, nor is much data available on either LLRD chemical make-up or size distributions in uranium mines and mills. This information is important to identify the main radioisotopes in LLRD, their concentration in air, and their size distribution as the latter determines the LLRD attachment characteristics in the respiratory system (1-3).

This report presents experimental data collected in a uranium mill. Long-lived radioactive dust is generated in the course of mechanical and physico-chemical unit operations carried out in the separation and refining processes of uranium, or uranium chemical compounds, from uranium ores.

The data in this report pertain to some physico-chemical milling operations. These include the following operations: acid leaching, counter-current decantation (CCD), solvent extraction, yellowcake precipitation and yellowcake drying. A study of mechanical unit operations in the same uranium mill, including yellowcake packaging, has been published elsewhere (4).

Measurements were conducted of LLRD and radon progeny associated with

dust in the 1-30 μm size range, and radon progeny in the submicron size range. A variety of other dust and radioactivity measurements were also carried out. This study was suggested by Atomic Energy Control Board (AECB) and was conducted under partial funding from the same organization.

EXPERIMENTAL APPARATUS AND METHODS

Size distribution analyses of radioactive dust, radioactive aerosol and dust were conducted by means of two 10-stage, radial slot-design, cascade impactors, model 210, manufactured by Sierra Instruments Inc. (U.S.A.), now Anderson. Both cascade impactors were operated with the last two ultrafine impactor stages removed. These two stages were eliminated at the expense of losing some size distribution information, but with the obvious benefit of substantially increasing the amount of dust collected on the remaining eight impactor stages.

Glass Fiber filters (47 mm diameter), with radial slot design similar to that of the cascade impactor stages, were used as substrates to collect the samples. The cascade impactors were operated for about 12 hours at a time at a sampling flow-rate of 10.5 L/min.

The Glass Fiber substrates placed behind the stages of the cascade impactors enabled determination of the size distribution (mass median aerodynamic diameter (MMAD), and geometric standard deviation) of dust by determining the weight of the filters before and after the sampling period. The substrates were dried before and after sampling to eliminate moisture. Ambient temperature and pressure were carefully noted during sampling and results were corrected according to standard operating procedures. Total dust was also estimated from cascade impactor data.

Radioactivity (α-particle) measurements on the impactor substrates also enabled calculation of the long-lived radioactive dust (LLRD), and radon

progeny, size distribution, i.e., activity median aerodynamic diameter (AMAD), and geometric standard deviation.

Also used in the determination of LLRD and radon progeny size distribution were two small, 8-stage, personal Marple cascade impactors (5). These impactors differ significantly from the Sierra impactors in a number of ways such as size, weight and geometry. The Marple impactors are much smaller and lighter than the Sierra impactors. The impactor stages slot design is also different, i.e., six radial slots for the Marple impactor as opposed to four radial slots for the Sierra impactors. The Marple impactors were operated at a nominal flow-rate of 2 L/min. Stainless steel substrates were used as dust collectors. Because of the low flow rate at which these impactors are operated and the relatively large weight of the substrates, as compared with Glass Fiber filters, no attempt was made to measure dust, only the radioactivity associated with it. The total LLRD and radon progeny concentrations were also estimated from impactor data. Radon progeny were measured 40 min after sampling. A counting time of 5 min was chosen. The α-particle activity of the LLRD was measured 1-2 weeks after sampling to allow the radon progeny and thoron progeny, if any, to decay away completely. Because of the low LLRD activity, each sample was counted several times for 30 min each time, and the average value, after subtracting the background, was used in the calculations.

The procedure used for the determination of dust, activity, and size distribution from the cascade impactor data was as follows:

1. Activity (dpm, i.e., disintegrations per min) and dust mass collected on each impactor stage were carefully noted.
2. Total activity and total dust mass from all the stages of the impactor, including the backfilter (BF), were estimated.
3. Percentage (%) activity and % dust mass for each impactor stage were

calculated.

4. Cumulative % of dust mass and cumulative % of activity, less than $D_{p,50}$ (see below), were estimated as follows. Dust mass (or activity) % of the BF was used as cumulative % for the last ultrafine stage, i.e., stage 8. The cumulative % for the next stage was obtained by adding the % of dust mass (or activity) to the cumulative % dust mass (or activity) corresponding to the previous stage, and so on.

5. Cumulative % dust mass (or activity), less than $D_{p,50}$, versus EAD was plotted.

The variable $D_{p,50}$ is defined as the particle cut-off at 50% collection efficiency for spherical particles. The magnitude EAD is the equivalent Aerodynamic Diameter defined as the size of a spherical particle of density 1 g/cm^3 which has the same terminal settling velocity as the sampled particle.

In addition to cascade impactors, total dust mass in the respirable size range was monitored with a continuous, optical system, dust sampler model Mini-Ram PDM-3, manufactured by Hoskins (U.S.A.).

Identification of long-lived radionuclides was done using α- and γ-spectrometry of several dust samples. Spectrometric analyses were carried out using a silicon-barrier detector (SiBD) spectrometer for α-spectrometry, and a high purity Germanium detector (HPGD) for γ-spectrometry.

Radon progeny Working Levels, WL, were measured for several physico-chemical operations using a continuous Working Level monitor model WLM-300 (EDA Instruments, Toronto), and by grab-sampling using the Thomas-Tsivoglou method. Radon gas concentrations were measured by grab-sampling using the scintillation cell method.

PHYSICO-CHEMICAL OPERATIONS

Several physico-chemical operations in the mill were monitored. Broadly speaking, this part of the mill circuit is as follows. The ground uranium ore from the rod and ball mills is treated with a neutral thickener. The neutral thickened slurry is treated with sulphuric acid, sodium chlorate and steam (acid leaching), and the leached slurry is directed to a series of counter-current decantation (CCD) tanks where the tailings are removed from the solution as a 55% solid slurry. Counter-current decantation of the liquid solution, containing the uranium-rich phase, is fed to a clarification plant where the solution is passed through several sand filters to remove any suspended solid matter. The clarified liquid solution is directed to a liquid-liquid extraction plant. The effluent from the CCD is neutralized with milk of lime and removed from the plant to a tailings pond.

The filtered/clarified uranium-compound liquid phase solution is treated with a mixture of kerosene, alcohol and an amine. Kerosene is used as a liquid carrier. The alcohol is employed to keep the amine dispersed in the liquid phase. The amine reacts chemically with the uranium compound and forms an organic complex which is subsequently stripped from the liquid solution by means of sodium chloride. The scrubbed raffinate is treated with milk of lime as indicated above.

The high grade uranium compound solution from the extraction process is treated with milk of magnesia where the uranium compound is precipitated as yellowcake. The yellowcake solution is thickened by settling and water evaporation. The yellowcake is dried in a dryer, stored in a yellowcake storage bin, and finally packaged in special drums in the yellowcake drying and packaging section.

Monitoring was carried out on the following mill operations: acid

leaching, counter-current decantation, solvent extraction, yellowcake precipitation, and for completeness, yellowcake packaging.

EXPERIMENTAL RESULTS AND DISCUSSION

Measurements were conducted during March and June 1986. Four cascade impactors were used, namely: the two Sierra impactors labelled EMR and C, and two Marple impactors labelled M_1 and M_2. All impactors were operated with 8-stages. The average operating characteristics of the impactors are shown in Table 1.

Because of the low sampling flow-rate of the Marple impactors, and the relatively low dust concentration in mill air at the time, no attempt was made to determine the dust mass on the different stages. Hence, no MMAD data from these impactors are available. Marple impactors were only used to gather radioactivity data to calculate the AMADs and the LLRD concentration in air.

The data obtained with the cascade impactors and other instrumentation have been summarized in Tables 2 to 5.

Table 2 shows cascade impactors data for long-lived radioactive dust and radon progeny. The data included are MMAD, AMAD, geometric standard deviations, dust concentration, LLRD concentration, and the specific radioactivity associated with dust. Table 2 shows the following features of practical interest:

1. The AMAD corresponding to the LLRD is, on average, larger than the corresponding MMAD of the carrier dust;
2. The largest values for AMAD and MMAD were found in the following operations: counter-current decantation (CCD), yellowcake precipitation, and yellowcake packaging. Acid leaching and solvent extraction had lower values for the above variables, particularly solvent extraction. The average values for MMAD and AMAD corresponding to the operations

indicated in Table 2 and given in Table 3.

3. Significant differences in the values of the AMAD were found in samples taken with the Sierra and Marple impactors. However, there are insufficient experimental data to quantify this statement unambiguously, and more work under controlled experimental conditions is necessary to compare the performance of the two types of impactors.
4. As expected, the AMAD corresponding to the radon progeny associated with dust was much less than its corresponding MMAD. The AMAD obtained was in the range 0.15 to 0.6 μm, essentially the same as that for the mechanical operations reported elsewhere (4). These data indicate that the radon progeny is preferentially associated with particulate matter of submicron size.
5. Except for the yellowcake packaging operation, airborne dust concentration in the 0.2 to 21 μm range was relatively low ($\leq$0.4 mg/m^3). Solvent extraction showed the lowest dust concentration (~0.06 mg/m^3).
6. As expected, the LLRD concentration was by far the highest for the yellowcake packaging operation followed by yellowcake precipitation, counter-current decantation and acid leaching. Despite the different air dilution factors between March and June, dust and radioactivity concentrations were much lower at the solvent extraction plant than for the rest of the other physico-chemical mill operations.
7. Calculation of the specific radioactive dust concentration activity (mBq/mg) shows that gross α-particle activity was not always linearly proportional to the amount of dust collected in the impactor substrates. It was found that the specific activity for a given operation decreased as the dust mass increased. These results suggest significant α-particle absorption in dust (see Table 2, yellowcake packaging). It should be noted that the specific activity for the yellowcake precipitation

operation calculated from data obtained in March and June differed by a factor 10 to 14. This large difference can only be attributed to differences in the grade of processed ore. This supposition was later confirmed by mill personnel, i.e., the grade of the ore processed in June was much lower than the grade processed in March. Notice, however, that the specific activity for the two experimental runs on March was quite close and within experimental error. The same applies to the two runs in June, with somewhat larger differences. This confirms that the grade of the ore during the March operations was constant. The same applies to June.

From item 7 and data from several mechanical operations reported elsewhere (4), it may be concluded that although relatively high dust mass is preferable to low dust mass for MMAD calculations, this may lead to substantial α-particle self-absorption and hence to underestimation of airborne radioactivity concentration. Furthermore, it may also lead to significant errors in the determination of AMAD. It is suspected that the contribution to the LLRD concentration (mBq/m^3), and its specific activity concentration (mBq/mg), for some cascade impactor stages may have been underestimated for milling operations that generated substantial amounts of dust.

Self-absorption problems can be minimized by choosing sampling times so as to ensure that adequate amounts of dust will be collected for accurate MMAD determinations, while at the same time consistent with the low α-particle absorption necessary for reliable measurements of the AMAD. It should be noted that during March, dust concentrations were much higher than in June when doors and windows in the mill remained open day and night.

Identification of the radionuclides in the radioactive dust was done by means of α-spectrometry and γ-spectrometry.

Alpha-spectrometry on at least one sample of each physico-chemical operation was carried out under vacuum conditions in order to improve the energy resolution of the spectra. Except for yellowcake samples, counting times in excess of 24 hours were necessary for good counting statistics.

Because of (a) self-absorption effects, i.e., α-particle absorption in dust, leading to spectrum broadening and photopeak overlapping; (b) relatively low signal-to-noise ratio; and (c) spectrometer drift, positive identification of the radionuclides in dust samples by α-spectrometry was not straightforward. A ^{241}Am source and a $^{226}Ra/^{232}Th$ source were used before and after each radioactive measurement of each dust sample. The radioactive sources listed below provided the following α-energy lines for α-particle identification and α-spectrometer calibration purposes:

$$^{241}Am \quad \overline{E}_{\alpha} = 5.45 \text{ MeV}$$

$$^{218}Po \quad E_{\alpha} = 6.0 \text{ MeV}$$

$$^{214}Po \quad E_{\alpha} = 7.69 \text{ MeV}$$

$$^{212}Po \quad E_{\alpha} = 8.78 \text{ MeV}$$

Alpha-spectra analyses showed two main photopeaks with the following energies: 3.99 ± 0.13 MeV and 4.46 ± 0.18 MeV. These two photopeaks can tentatively be ascribed to ^{238}U (4.2 MeV) and $^{234}U/^{230}Th$ (4.7 MeV), see Table 4. The lower α-particle energy measured for these radioisotopes is attributed to energy degradation in dust, i.e., self-absorption. Only these two peaks appear in the spectra corresponding to yellowcake precipitation, solvent extraction and yellowcake packaging. Counter-current decantation and acid leaching spectra also show a much smaller photopeak of higher energy which could not be unambiguously identified.

The radioisotope identification indicated above assumes no thorium present in the dust samples. This assumption is supported by open-face radon progeny grab-sampling measurements 40 min and 7 h after sampling. These

measurements showed negligible residual α-activity after the radon progeny decayed away.

Figure 2 shows two α-particle spectra corresponding to samples collected, respectively, during yellowcake precipitation and packaging operations. Table 4 shows the α-particle energy corresponding to the Uranium and Thorium natural series.

Dust samples from all the mill operations were analyzed by γ-spectrometry. However, despite the very high resolution of the apparatus (0.5 keV/channel), positive identification of the radionuclides in the dust samples was rather difficult even after counting for extended periods. The reason for this is the low radioactivity in the samples and the relatively large natural background. The activity of the samples is related to the sampling time which determines the amount of dust collected at a given flow-rate, and the ore grade.

Because of the relatively large amount of dust generated in yellowcake packaging, the activity of the samples from this operation was easily measurable and the radioisotope make-up could be quite confidently identified. The following radioisotopes were identified: ^{234}Th, ^{234m}Pa, ^{234}U, ^{230}Th and some ^{226}Ra, ^{210}Pb and ^{235}U. The radioisotope composition for other operations was similar but the activity considerably smaller, a fact that made identification somewhat difficult at times. Table 5 shows γ-ray energies corresponding to some radioisotopes of interest in the natural uranium radioactive chain.

Figures 3 to 14 show the cumulative dust mass percentage and/or α-particle cumulative activity percentage, of size less than $D_{p,50}$, versus $D_{p,50}$ for several cascade impactors. Four physico-chemical operations were monitored, i.e., acid leaching, counter-current decantation, solvent extraction and yellowcake precipitation and drying.

Although the meaning of MMAD and AMAD has been explained above, the labels MMAD and AMAD, that appear in the graphs, are also used here to identify, respectively, dust size distribution and radioactivity size distribution curves. The graphs drawn through direct experimental data points represent straight lines calculated by linear regression analysis. Two radioactivity size distribution graphs are sometimes shown for the Sierra impactors. In one (AMAD), data from the last three cascade stages have been ignored. The other graph, labelled $\overline{\text{AMAD}}$, has been obtained taking into account all impactor stages. The difference between both graphs at the AMAD point (i.e., 50% cumulative ordinate) is ~10%. In most cases, however, AMAD and $\overline{\text{AMAD}}$ roughly coincide, and hence only one graph is shown.

Except for data obtained with the Marple impactors, upper graphs refer to long-lived radioactive dust, whereas lower graphs refer to radon progeny (RnD), e.g., Figure 3.

Figures 3 and 4 show data for two acid leaching operations carried out on different days. Data were obtained with the same Sierra cascade impactor at the same location. The graphs show the cumulative dust mass percentage and α-particle cumulative activity percentage versus $D_{p,50}$. Data were as follows: MMAD = 6.9 (7.4) μm, AMAD (LLRD) = 6.5 (8.5) μm, $\overline{\text{AMAD}}$ (LLRD) = 6.6 (9.5) μm, and AMAD (RnD) = 0.24 (0.17) μm. The data in round brackets correspond to the second day. The data show that the AMAD for LLRD and RnD for the two days differed by about 40%. However, the only difference between the two tests was the length of the sampling period, i.e., first test lasted about 12 hours and was carried out during the day shift (7:47 to 19:37) whereas the second test lasted about 22 hours (from June 7 at 9:50 to June 8 at 7:20), and hence, was carried out through the day and night shifts.

Figure 5 shows data for the counter-current decantation (CCD) operations at two different locations in the CCD plant. Data were obtained

with two different Marple cascade impactors. The AMAD (LLRD) obtained were 12.8 μm and 10.5 μm, with an average of ~11.6 μm. The difference between these two experiments are considered to be within experimental error. Also shown in Figure 5 is the corresponding AMAD for the radon progeny, RnD. The values obtained were 0.15 μm and 0.33 μm, corresponding respectively, to an AMAD (LLRD) of 12.8 μm and 10.5 μm, as indicated above. The large difference between those two values for the AMAD (RnD) is not surprising because of the relatively low short-lived α-particle activity counted, in the presence of relatively large backgrounds and LLRD corrections, and the short counting times that were necessary to measure the activity on the substrates before substantial radioactive decay took place.

Figure 6 shows similar data to Figure 5 (i.e., Marple impactor), but for a different location in the CCD plant. Data for the AMAD were as follows: AMAD(LLRD) = 13.1 μm and AMAD (RnD) = 0.11 μm. The average value for the AMADs calculated from Figures 5 and 6 and Table 2 are as follows: $AMAD(LLRD)_{av} = 12.1 \pm 1.4$ μm and $AMAD(RnD)_{av} = 0.2 \pm 0.1$ μm.

The data from Figures 5, 6 and 14, obtained with the Marple impactors, show an unusual curve-shaped size distribution for the LLRD which is not shown for the case of the radon progeny. The shape of the LLRD distributions obtained with these impactors cannot be explained satisfactorily at present.

Figure 7 shows more data for the CCD operation obtained this time with a Sierra cascade impactor. Examination of Figures 5 to 7 show that the data obtained with the two types of cascade impactors for CCD operations is quite consistent. An overall average for this operation taking into account all data from the Sierra and Marple impactors gives AMAD (LLRD) = 11.6 $\pm$ 1.5 μm, AMAD (RnD) = 0.20 $\pm$ 0.10 μm.

Figures 8 and 9 show data for solvent extraction operations obtained the same day with a Sierra cascade impactor (Figure 8), and a Marple cascade

impactor (Figure 9). These Figures show that AMAD (LLRD) did not differ significantly for these two impactors, i.e., 4.5 μm and 3.8 μm, respectively, with an average of 4.15 μm. The AMAD (RnD), however, differed substantially, i.e., 0.4 μm and 0.58 μm (>40% difference) with an average of 0.49 μm. Notice that data from the first impactor stages have been ignored because no, or very little, radon progeny activity was associated with particulate matter above ~2 μm.

Figures 10 to 14 show data obtained with different cascade impactors (Sierra and Marple), on different days and at different locations for yellowcake precipitation operations.

Figures 10 and 11 show data for the same Sierra impactor for two different days. Although all graphs refer to the yellowcake operation, in one case sampling was conducted during the drying phase of the operation (Figure 11), whereas in the other case sampling was carried out below the yellowcake precipitation reactor (Figure 10). This may explain the differences in AMAD (LLRD) observed. Independently from the sampler location, the above Figures show that AMAD (LLRD) was substantially higher in both cases than its corresponding MMAD. The AMAD for the radon progeny (See Figure 10) was about 0.40 μm.

Figures 12 and 13 also show as Figures 10 and 11 that the AMAD (LLRD) for the yellowcake precipitation operation was significantly higher than the MMAD of the carrier dust. The AMAD for the radon progeny was between 0.18 μm and 0.27 μm. An examination of the data from Figures 10 to 13 and Table 2 show a wide range of values for both the AMAD and MMAD. Values obtained in March were higher than values measured in June. The ratio of the maximum value to the minimum value for the AMAD and MMAD was greater than 2. It is not clear whether these differences are related to some difference in the characteristics of the uranium ore processed in March and June. It should be

noted that the lowest values obtained were below the yellowcake precipitation reactor.

Figure 14 shows AMAD data for the yellowcake precipitation obtained with a Marple cascade impactor. The graph shows the corrected and non-corrected size distributions. As indicated above, the shape of the distribution is not clearly understood.

Figure 15 shows radon progeny Working Level measurements conducted with a continuous Working Level monitor model WLM-300 manufactured by EDA Instruments (Toronto). In general, the Working Level (WL) measured was low, i.e., it rarely exceeded 50 mWL, and for short periods of time. The highest measured WL was during yellowcake precipitation and acid leaching operations. Lower radiation levels were measured at other locations and operations. The lowest WL measurements were in counter-current decantation and in solvent extraction operations.

Figure 16 shows the respirable dust concentration (mg/m^3) measured during several physico-chemical operations with a real-time, passive, continuous dust monitor model Mini-Ram PDM-3 manufactured by Hoskins (U.S.A). Three operations were monitored: counter-current decantation, acid leaching and yellowcake precipitation. The dust concentration was highly variable but was in general below 1 mg/m^3. The lowest dust concentration was found in yellowcake precipitation. Apart from the three operations indicated above, no other physico-chemical operations were monitored with the Mini-Ram.

SUMMARY AND CONCLUSIONS

From the data presented in this study the following conclusions can be drawn. Except for solvent extraction, the AMAD corresponding to the long-lived radioactive dust was larger than the corresponding MMAD of the carrier dust.

The MMAD and AMAD calculated for the dust cloud depended on the type of physico-chemical operation in the mill. The values for these two diameters were in the range 3 to 16 μm.

The AMAD corresponding to the radon progeny was in the submicron range, i.e., 0.11 to 0.58 μm.

Differences were found for the MMAD and AMAD obtained at the same location with different types of cascade impactors.

The respirable dust concentration and the long-lived radioactive dust concentration depended on the physico-chemical operation. Furthermore, these concentrations were lower during June than during March indicating processing of a lower ore grade and added ventilation because of the warmer weather.

ACKNOWLEDGEMENTS

This study was requested and partly supported by Atomic Energy Control Board (AECB). The authors are particularly grateful to Dr. H. Stocker and Dr. P. Duport for their interest and support in this work. The author would also like to thank Mr. T. Meadley (AMOK Ltd., Saskatoon) for his cooperation throughout this study. Finally, the authors would like to acknowledge the assistance of some of the staff at Cluff Lake Mining during this field investigation.

REFERENCES

1. Bigu, J. and Grenier, M.G., "Studies of radioactive dust in Canadian uranium mines"; CIM Bull, vol. 77, pp 62-68; 1984.

2. Duport, P.J. and Edwardson, E., "Characterization of radioactive long-lived dust present in uranium mine and mill atmospheres"; in Proc Occup

3. Bigu, J. and Grenier, M.G., "Characterization of radioactive dust in Canadian underground uranium mines"; Proc 2nd Ventilation Congr, Reno, Nevada, pp 269-277; A.A. Balkema, Rotterdam, P. Mousset-Jones (Ed.); 1985.

4. Bigu, J. and Edwardson, E., "Characterization of long-lived radioactive dust clouds generated in mechanical operations in a uranium mill"; Division Report M&ET/MRL 86- (TR), CANMET, Energy, Mines and Resources Canada; October 1986.

5. Hinds, W.C., Liu, W.V. and Froines, J.R., "Particle bounce in a personal cascade impactor"; Am Ind Hyg Assoc J, vol 46, No. 9, pp. 517-523; 1985.

Table 1 - Cascade impactors average operating characteristics

Impactor	Sampling Flow-Rate L/min	Stage Number	Cut-Off Size μm
EMR & C	10.5	1	14.91
		2	8.89
		3	3.58
		4	2.15
		5	1.36
		6	0.75
		7	0.41
		8	0.23
M_1 & M_2	2.0	1	21.3
		2	14.8
		3	9.8
		4	6.0
		5	3.5
		6	1.6
		7	0.93
		8	0.52

Table 2 - Cascade impactors data for several physico-chemical operations in a uranium mill.

Operation	Date	Impactor	MMAD (μm)	Dust σg	AMAD(LLRD) (μm)	LLRD σg	AMAD(RnD) (μm)	RnD σg	Dust Conc. mg/m^3	LLRD Conc. mBq/m^3	LLRD(S.A.) mBq/mg
Acid Leaching	June 5	C	6.9	2.4	6.6	3.5	0.24	4.0	0.30	252	840
" "	June 7	C	7.4	2.8	9.5	4.0	0.17	4.2	0.23	181	787
Counter-Current Decantation (CCD)	June 7	EMR	8.3	3.0	10.2	3.6	0.21	3.0	0.40	266	665
	June 5	M_1	-	-	12.8	1.7	0.15	33.0	-	394	-
"	June 5	M_2	-	-	10.5	1.8	0.33	16.0	-	371	-
"	June 6	M_1	-	-	13.1	1.8	0.11	14.7	-	160	-
Solvent Extraction	June 6	EMR	4.5	5.3	2.9	3.7	0.40	3.3	0.06	39	650
" "	June 6	M_2	-	-	3.8	3.9	0.58	2.8	-	31	-
Yellowcake Precip.	March 27	C	7.0	4.0	16.2	3.8	0.27	5.0	0.34	2110	6206
" "	March 27	EMR	9.0	2.8	13.2	3.6	0.18	8.3	0.31	1890	6097
" "	June 8	C	5.4	6.3	9.0	4.7	-	-	0.30	134	447
" "	June 7	M_1	-	-	13.2	1.8	-	-	-	106	-
" "	June 6	C	4.0	3.8	6.6	4.9	0.40	10.8	0.06	35	583
Yellowcake Packaging	March 22	C	10.5	3.1	11.1	3.5	-	-	12.43	1.30×10^5	1.05×10^4
" "	March 22	EMR	12.3	3.7	11.8	2.6	-	-	6.21	1.25×10^5	2.01×10^4

Notes: a) C and EMR are Sierra impactors; M_1 and M_2 are Marple impactors.
b) σg represents geometric standard deviation.
c) RnD stands for radon progeny.
d) S.A. indicates specific activity.
e) Yellowcake packaging data have been included for completeness.

Table 3 - Average values of MMAD and AMAD for different mill operations.

Mill Operation	MMAD μm	AMAD μm
Acid leaching	7.15	8.05
CCD	8.3	11.65±1.51
Solvent extraction	4.5	3.35
Yellowcake precipitation	6.35±2.15	11.64±3.8
Yellowcake packaging	11.4	11.45

Table 4 - Alpha-particle energy corresponding to some members of the uranium and thorium natural radioactive chains.

Radioisotope	Symbol	α-Energy MeV	Remarks
Thorium	^{232}Th	4.08	Long-lived
Thorium	^{228}Th	5.52	" "
Radium	^{224}Th	5.79	" "
Thoron	^{220}Rn	6.28	Short-lived
Thorium A	^{216}Po	6.80	" "
Thorium C	^{212}Bi	6.05	" "
Thorium C'	^{212}Po	8.78	" "
Uranium	^{238}U	4.2	Long-Lived
Uranium	^{234}U	4.7	" "
Thorium	^{230}Th	4.7	" "
Radium	^{226}Ra	4.8	" "
Radon	^{222}Rn	5.49	Short-lived
Radium A	^{218}Po	6.0.	" "
Radium C'	^{214}Po	7.68	" "
Radium F	^{210}Po	5.30	" "

Table 5 - Gamma-energy of some of the radioisotopes identified in dust samples from several mill operations*

Radioisotope	Symbol	γ-Energy keV	Remarks
Lead	^{210}Pb	46.50	Long-lived (medium)
Thorium	^{234}Th	63.29	Long-lived
		92.38	"
		92.80	"
Thorium	^{230}Th	67.73	Long-lived
		143.60	"
		185.80	"
Uranium	^{234}U	53.00	
Uranium	^{235}U	84.24	Long-lived
		143.76	"
		185.71	"
		205.00	"
Radium	^{226}Ra	185.99	Long-lived
Palladium	^{234m}Pa	1001.40	Long-lived

*Not all the gamma energies shown in the Table have been identified. ^{226}Ra, ^{210}Pb and ^{235}U identification is tentative.

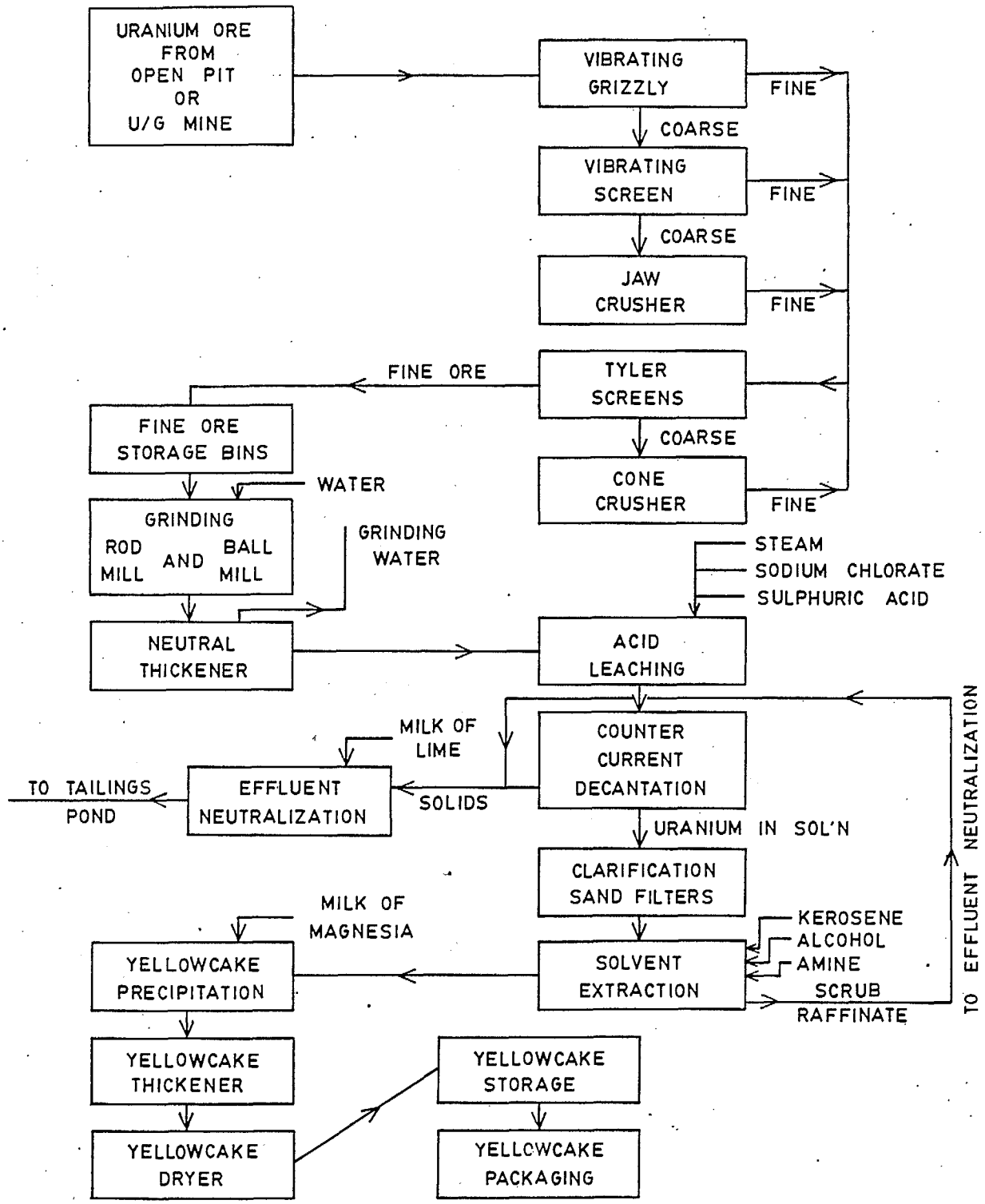

Fig. 1 - Block diagram of mechanical and physico-chemical operations in a uranium mill.

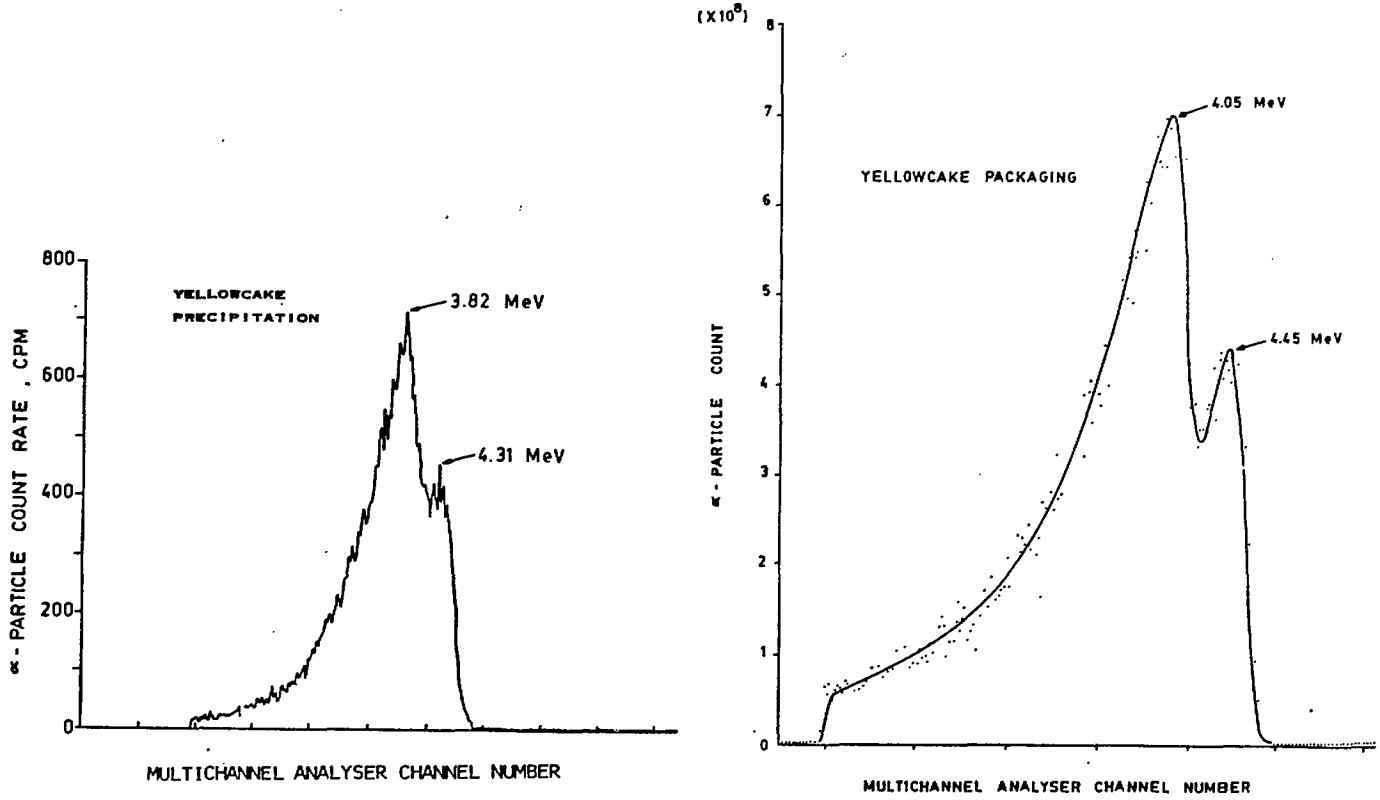

Fig. 2 - Alpha-particle spectra corresponding to different mill operations.

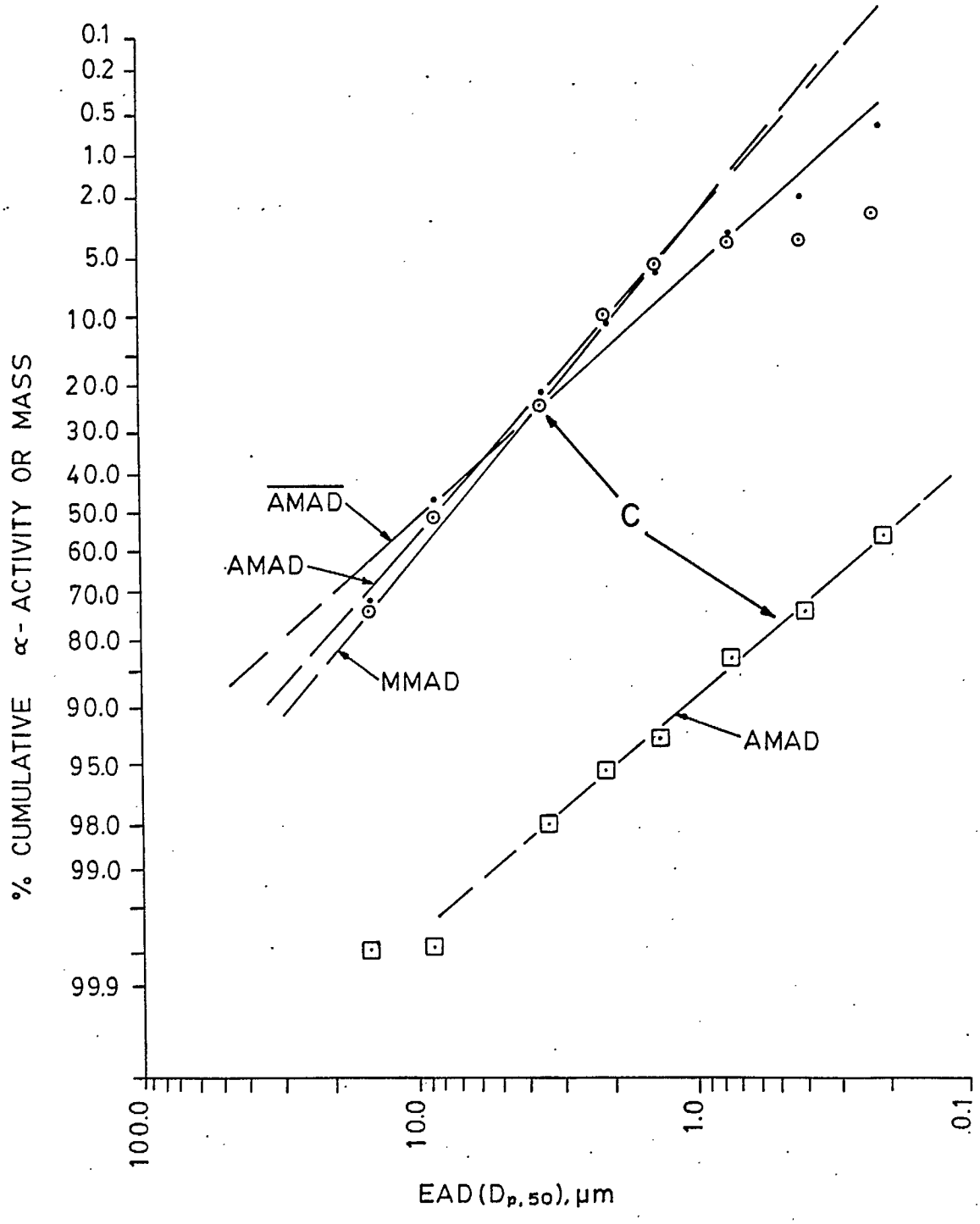

Fig. 3 - Percentage cumulative dust (MMAD), and percentage cumulative LLRD (AMAD), upper graphs, and radon progeny (lower graph) α-activity versus EAD for acid leaching.

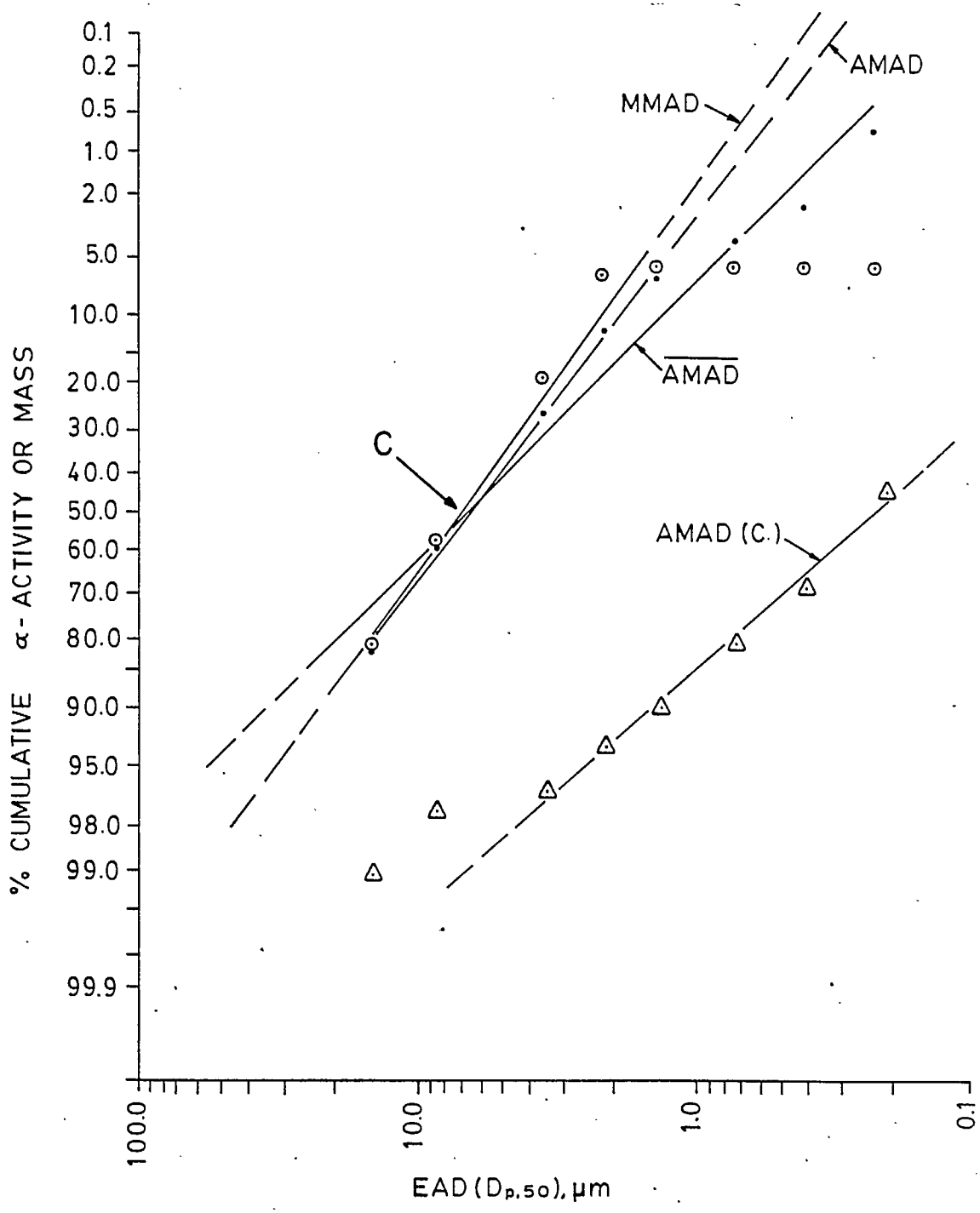

Fig. 4 - Percentage cumulative dust (MMAD), and percentage cumulative LLRD (AMAD), upper graphs, and radon progeny (lower graph) α-activity versus EAD for acid leaching.

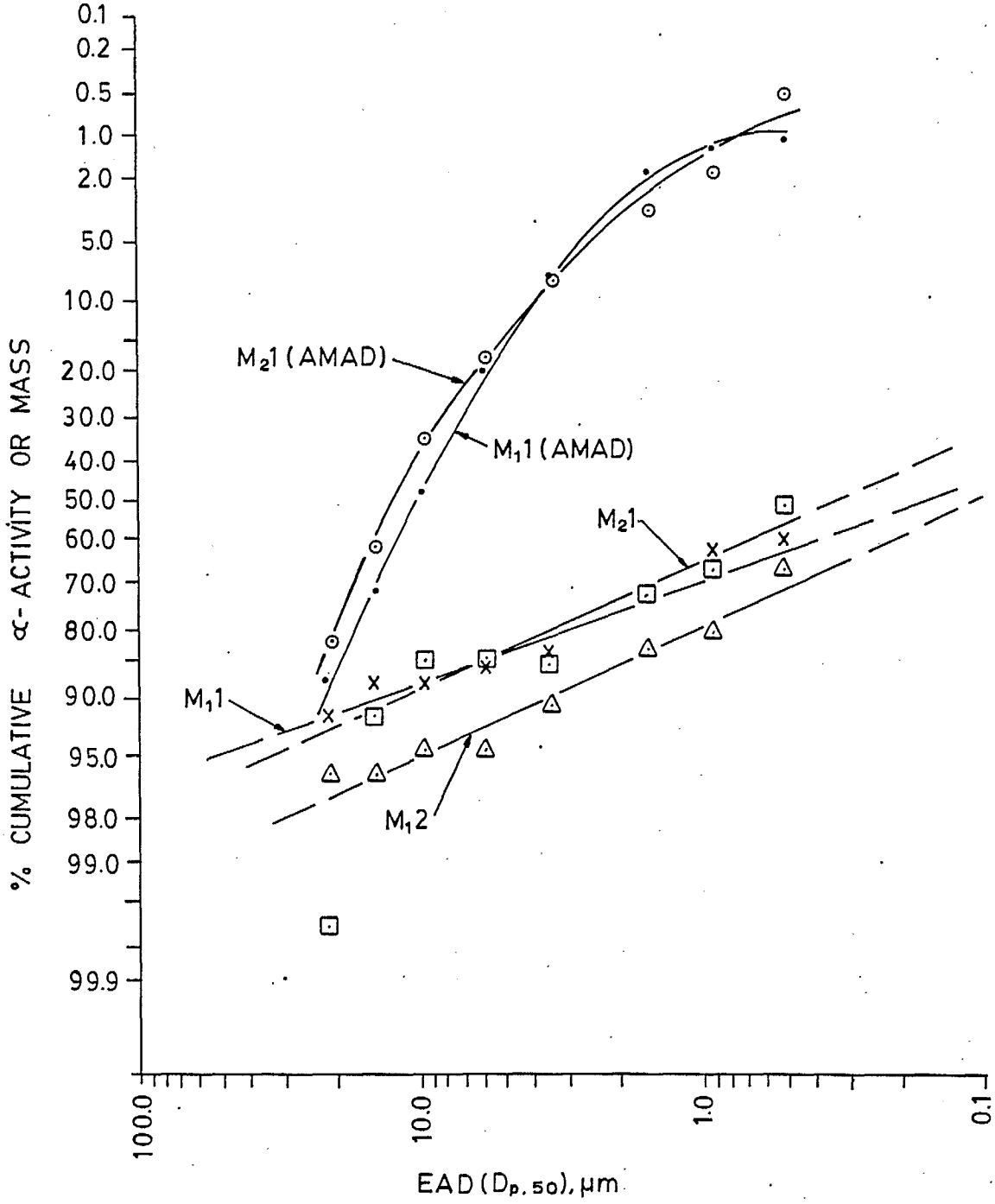

Fig. 5 - Percentage cumulative LLRD (upper graphs) and radon progeny (lower graphs) α-activity versus EAD for counter-current decantation operations. The numbers in M indicate the impactor and experimental run.

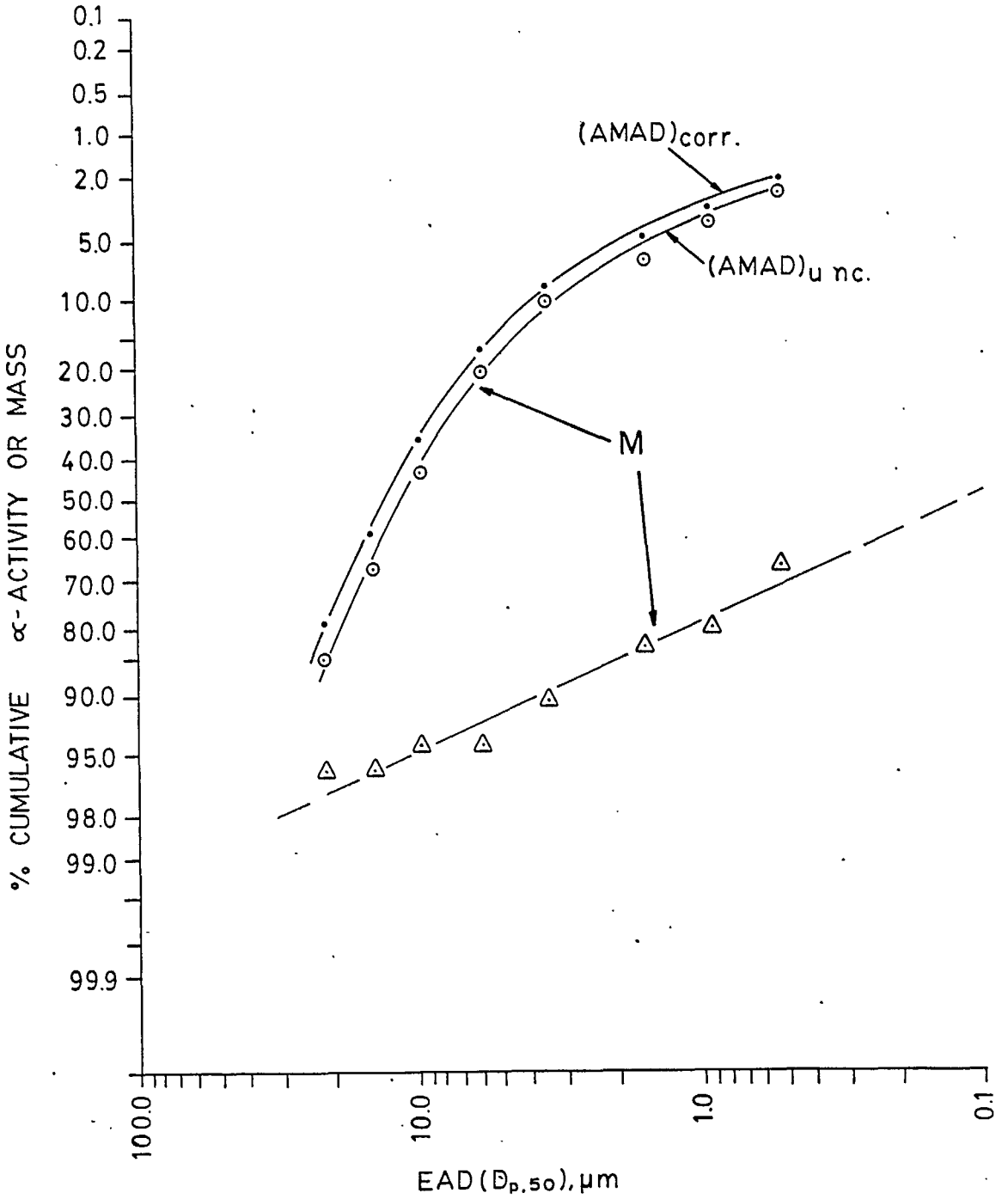

Fig. 6 - Percentage cumulative LLRD (upper graphs) and radon progeny (lower graph) α-activity versus EAD for counter-current decantation operations. (Note: the label corr. is used to indicate data corrected to take into account the collection efficiency of the different Marple impactor stages. Uncorrected data are indicated by the label unc.)

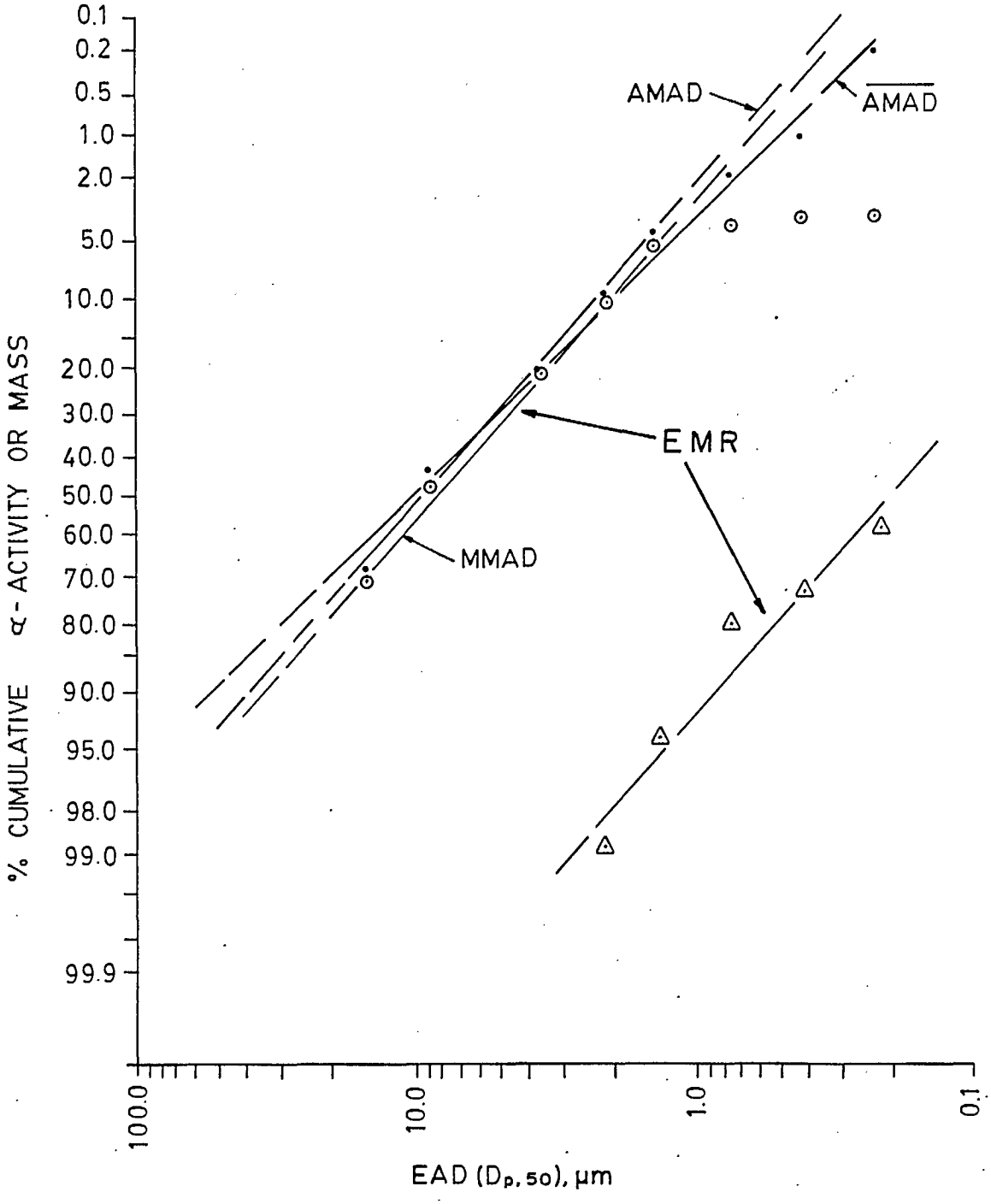

Fig. 7 - Percentage cumulative dust (MMAD), and percentage cumulative LLRD (AMAD), upper graphs, and radon progeny (lower graph) α-activity versus EAD for counter-current decantation operations.

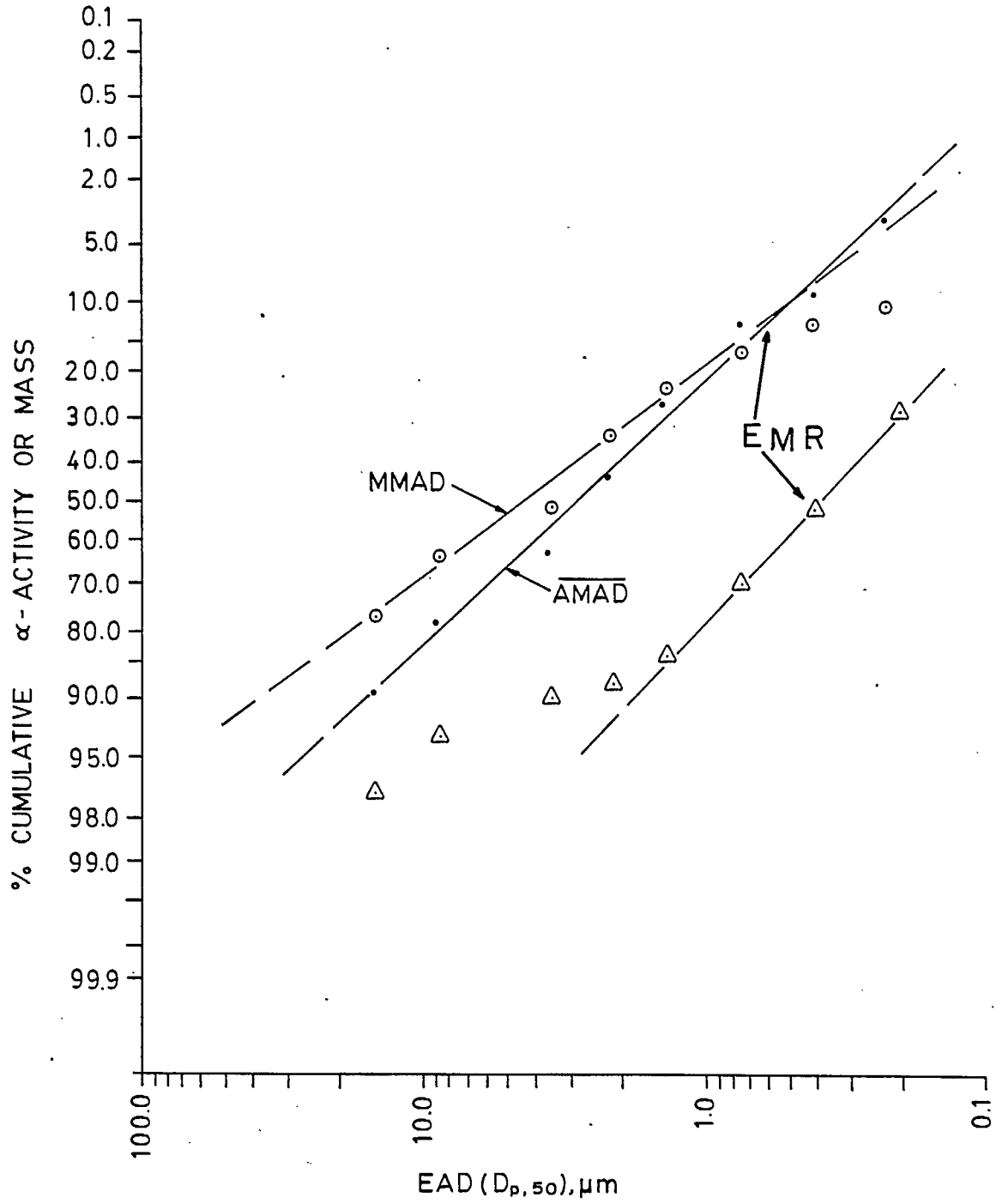

Fig. 8 - Percentage cumulative dust (MMAD) versus EAD, and percentage cumulative LLRD (AMAD) and radon progeny (lower graph) α-activity versus EAD for solvent extraction.

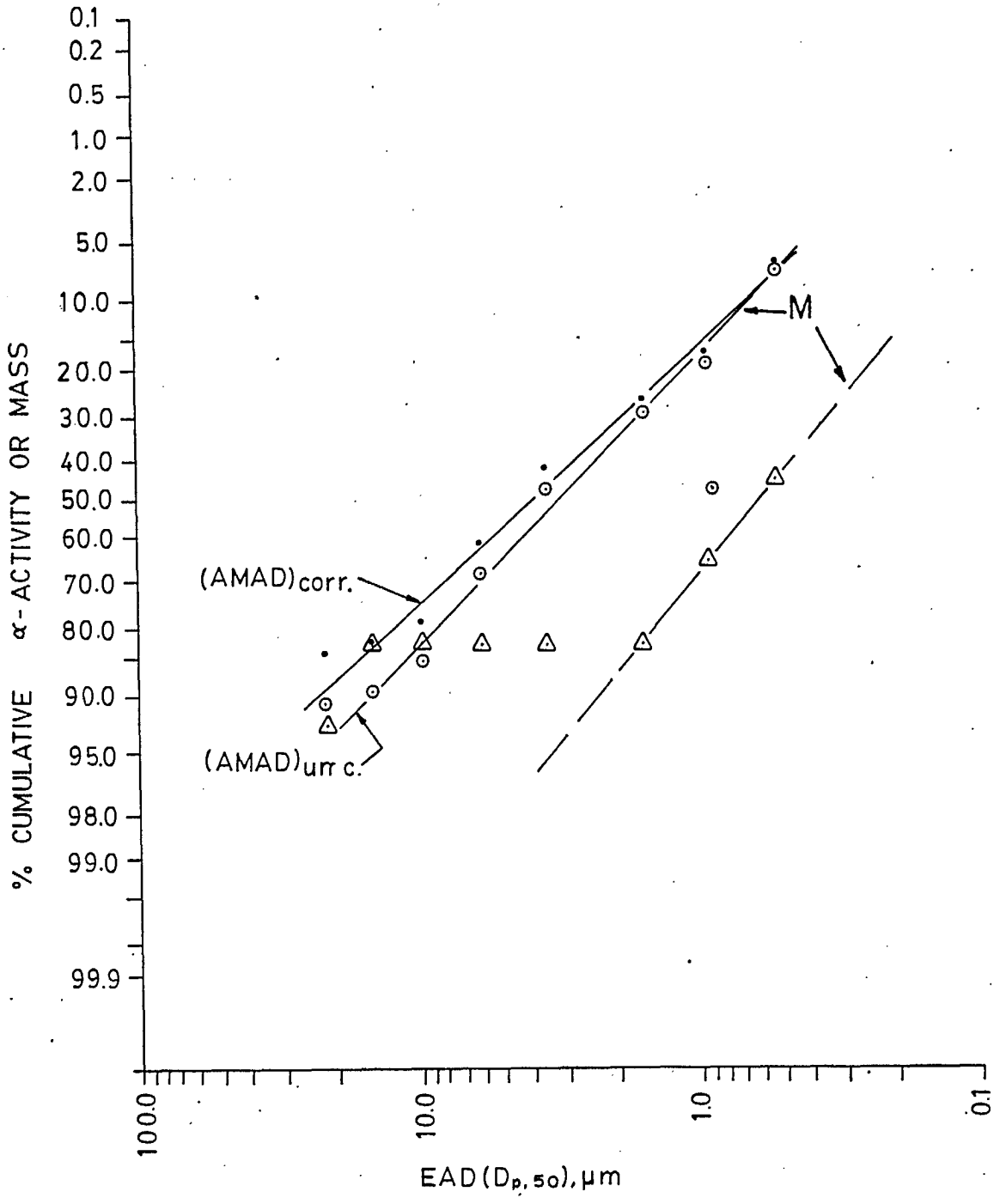

Fig. 9 - Percentage cumulative LLRD (upper graphs) and radon progeny (lower graph) α-activity versus EAD for solvent extraction. (Note: the label corr. is used to indicate data corrected to take into account the collection efficiency of the different Marple impactor stages. Uncorrected data are indicated by the label unc.)

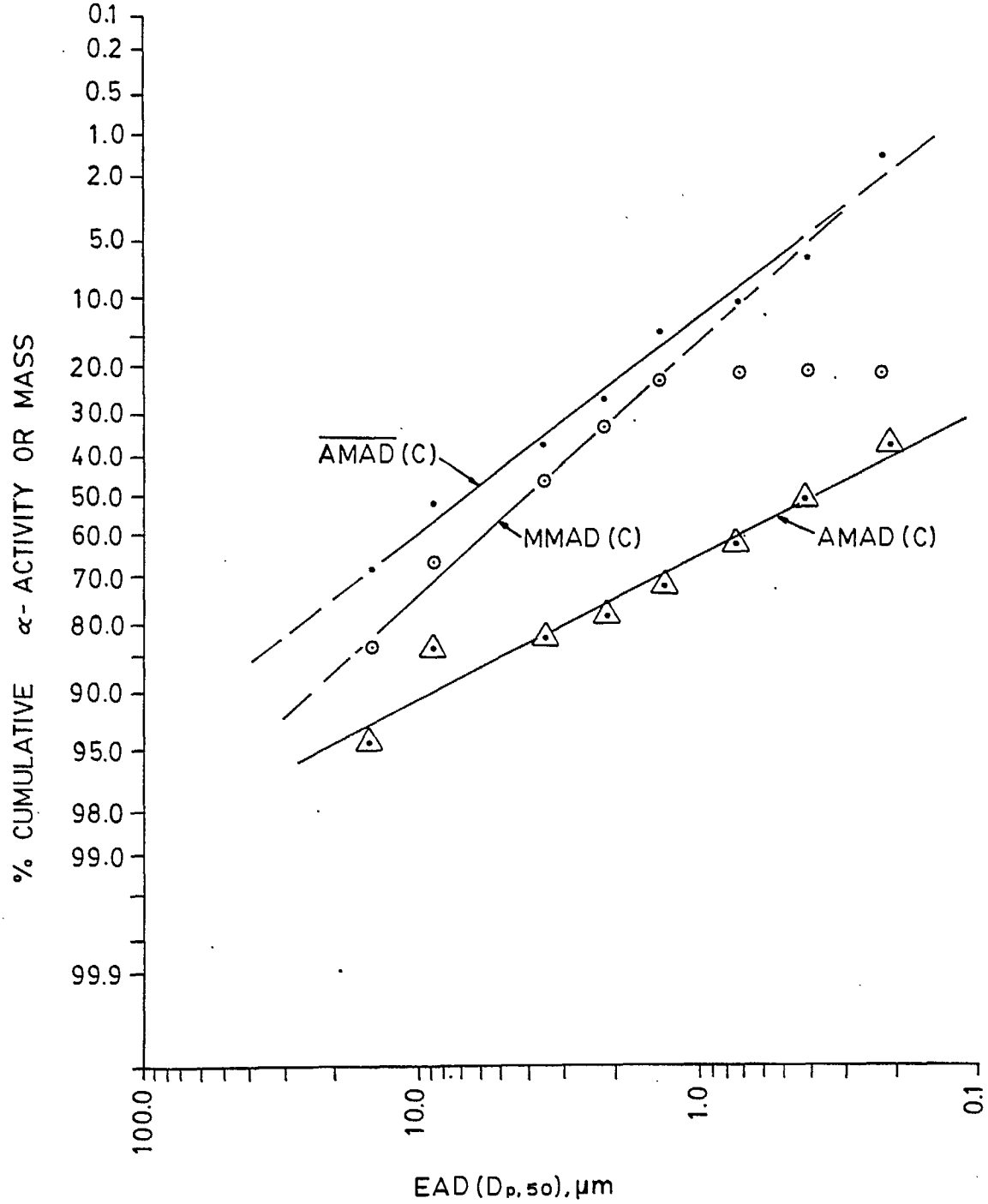

Fig. 10 - Percentage cumulative dust (MMAD) versus EAD, and percentage cumulative LLRD (AMAD), upper graph, and radon progeny (lower graph) α-activity versus EAD for yellowcake precipitation.

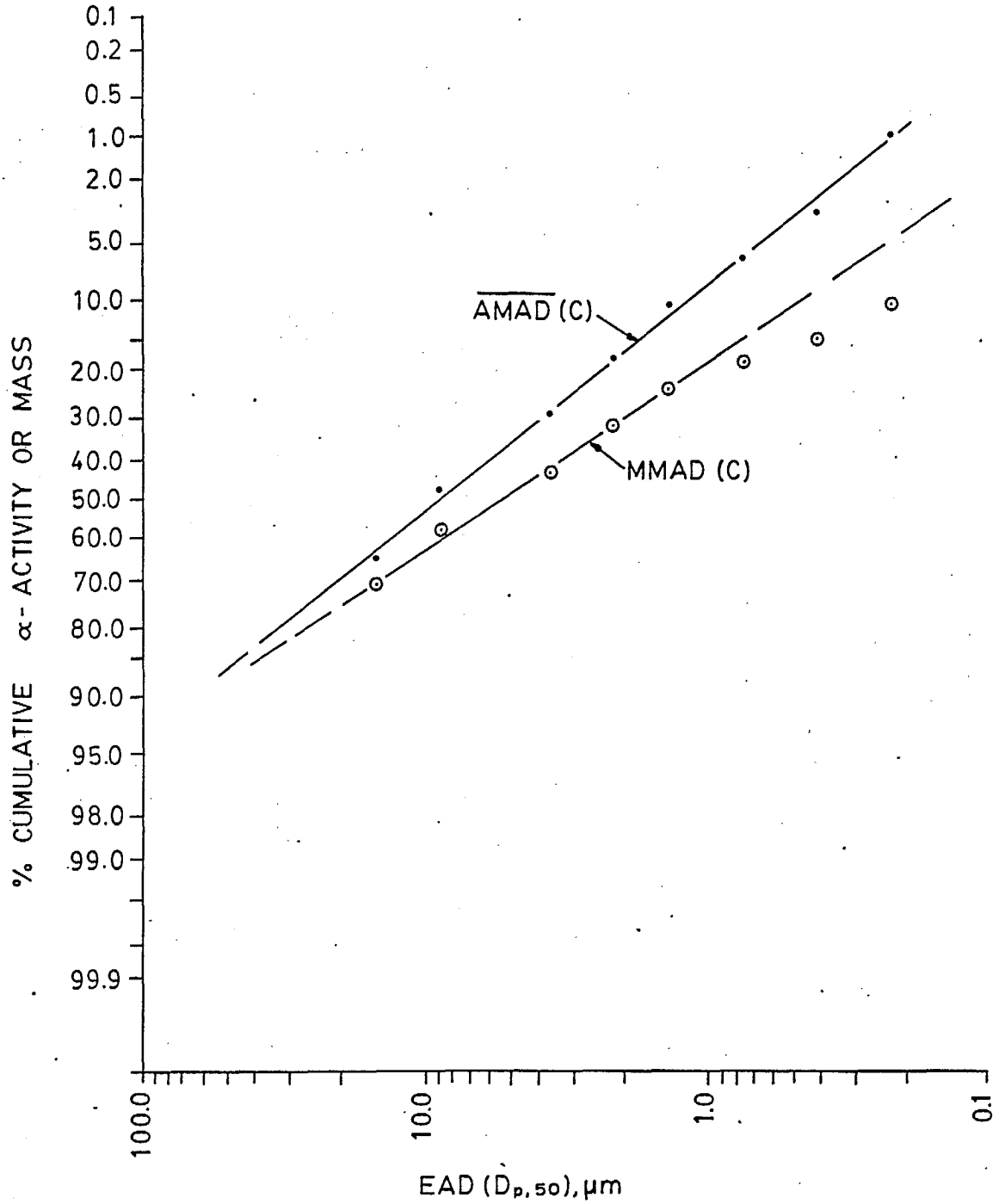

Fig. 14 - Percentage cumulative dust (MMAD) and LLRD (AMAD) α-activity versus EAD for yellowcake precipitation during the drying phase.

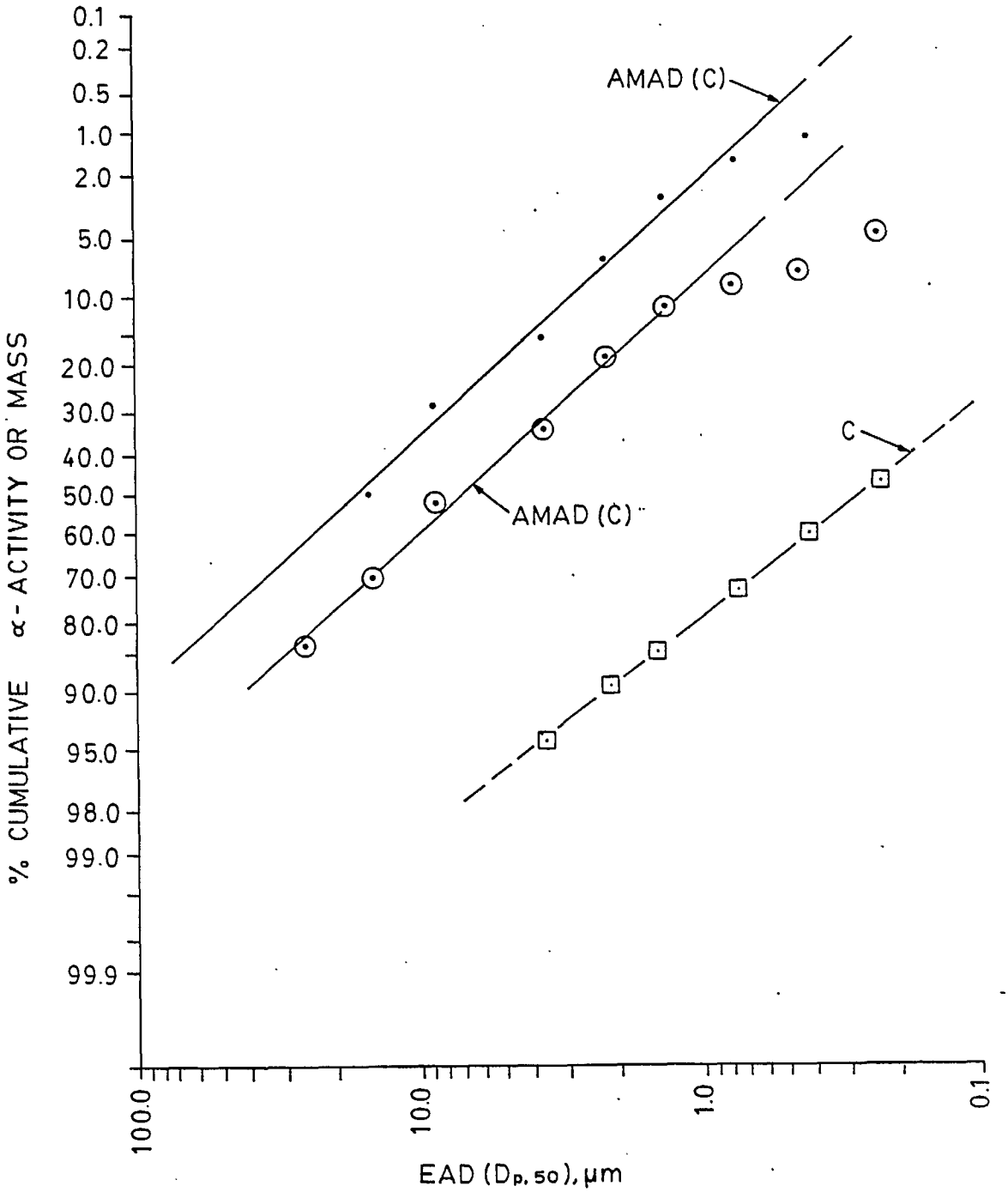

Fig. 12 - Percentage cumulative LLRD (upper graphs) and radon progeny (lower graph) α-activity versus EAD for yellowcake precipitation.

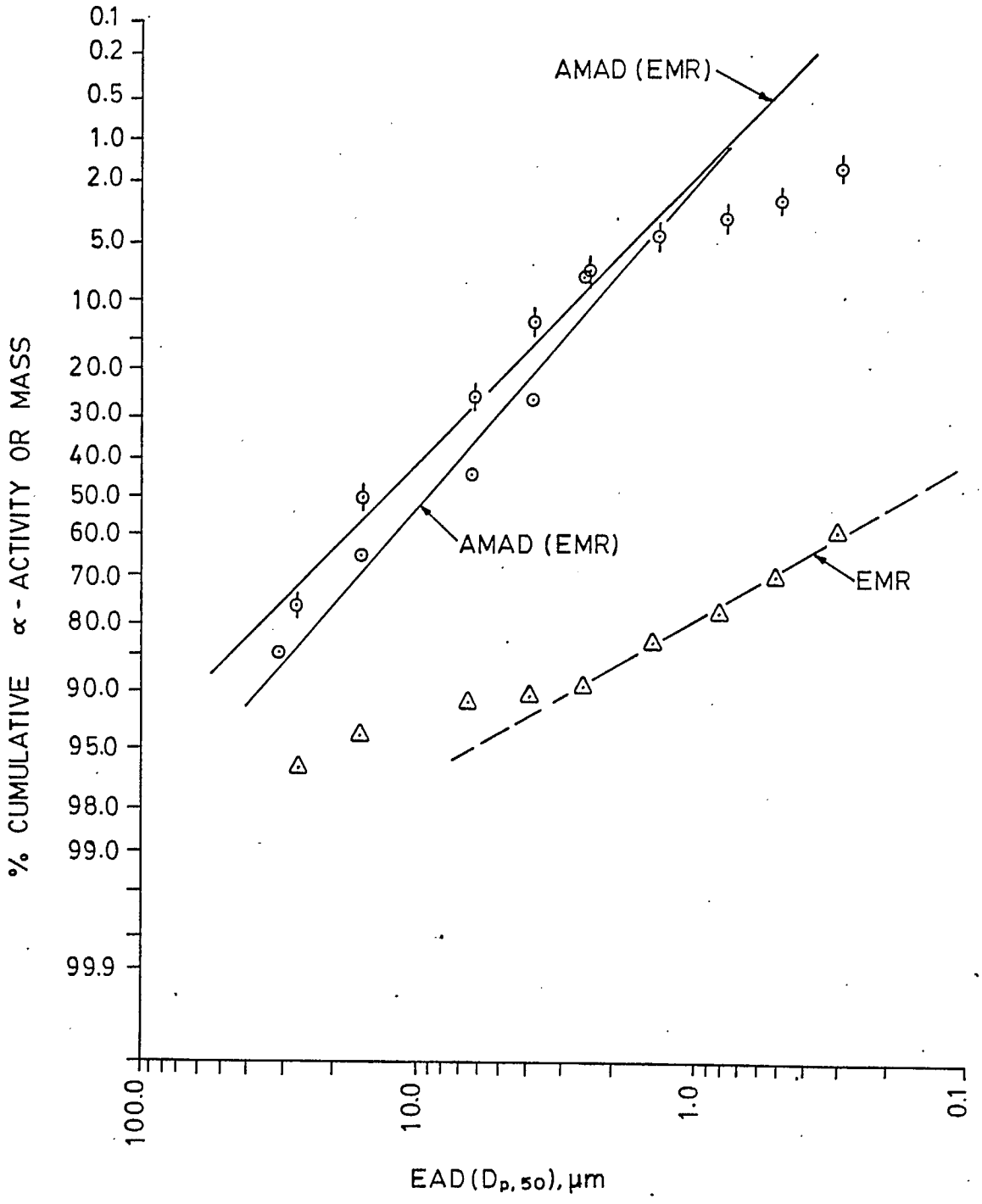

Fig. 13 - Percentage cumulative LLRD (upper graphs) and radon progeny (lower graph) α-activity versus EAD for yellowcake precipitation.

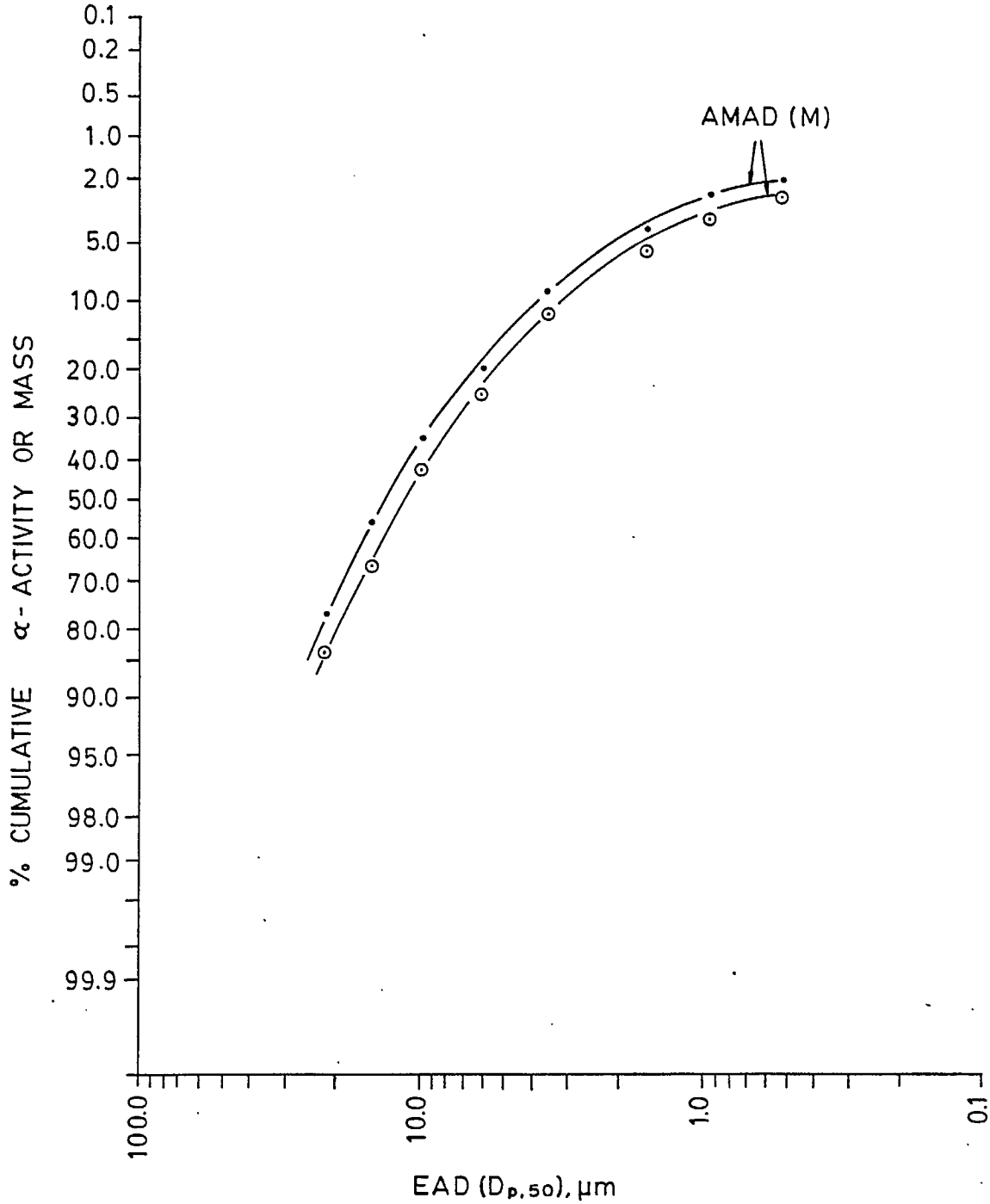

Fig. 14 - Percentage cumulative LLRD α-activity versus EAD for yellowcake precipitation. (Note: upper graph has been corrected for impactor stage collection efficiency. The lower graph shows non-corrected values.)

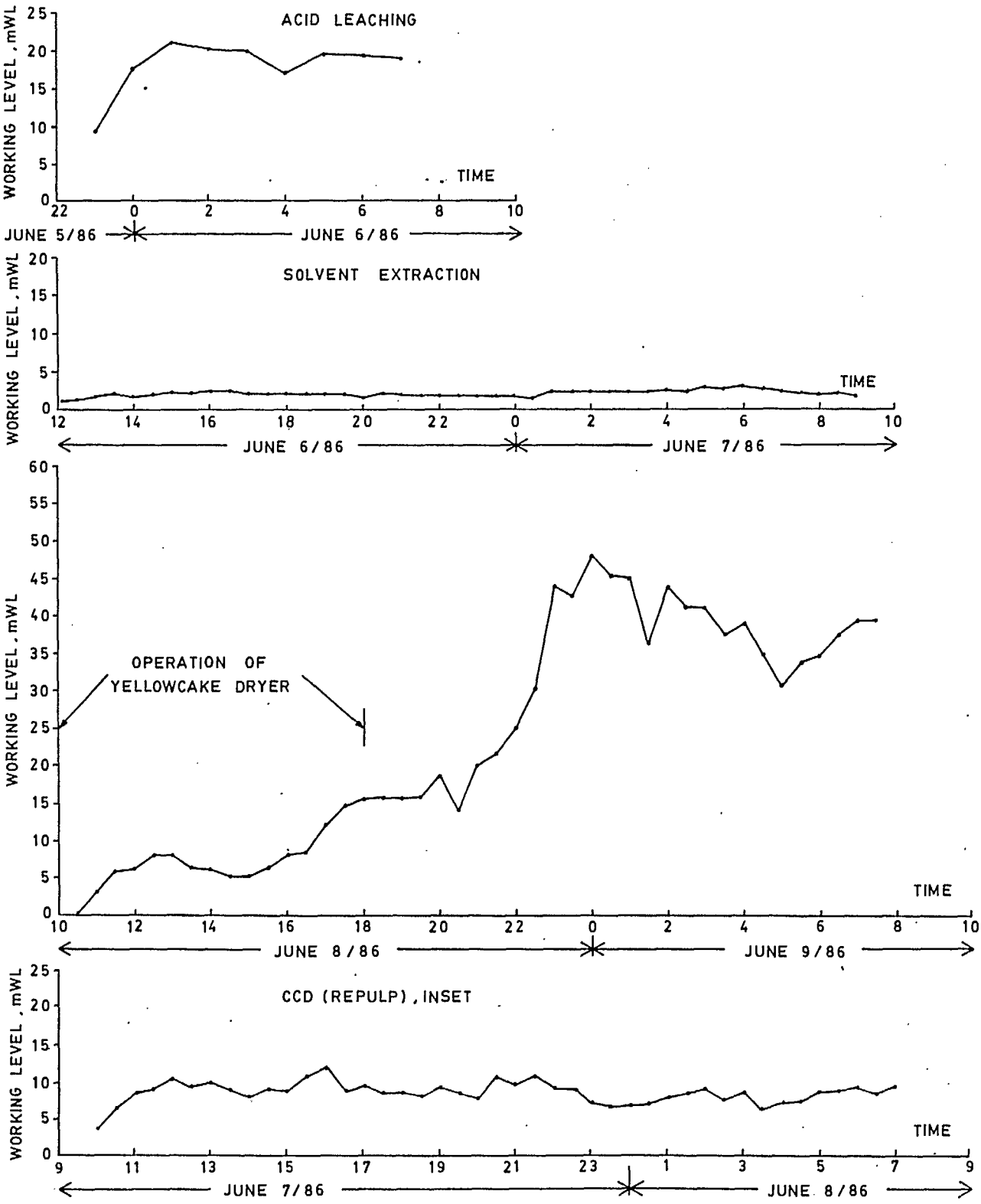

Fig. 15 - Radon progeny Working Level versus time for several physico-chemical operations.

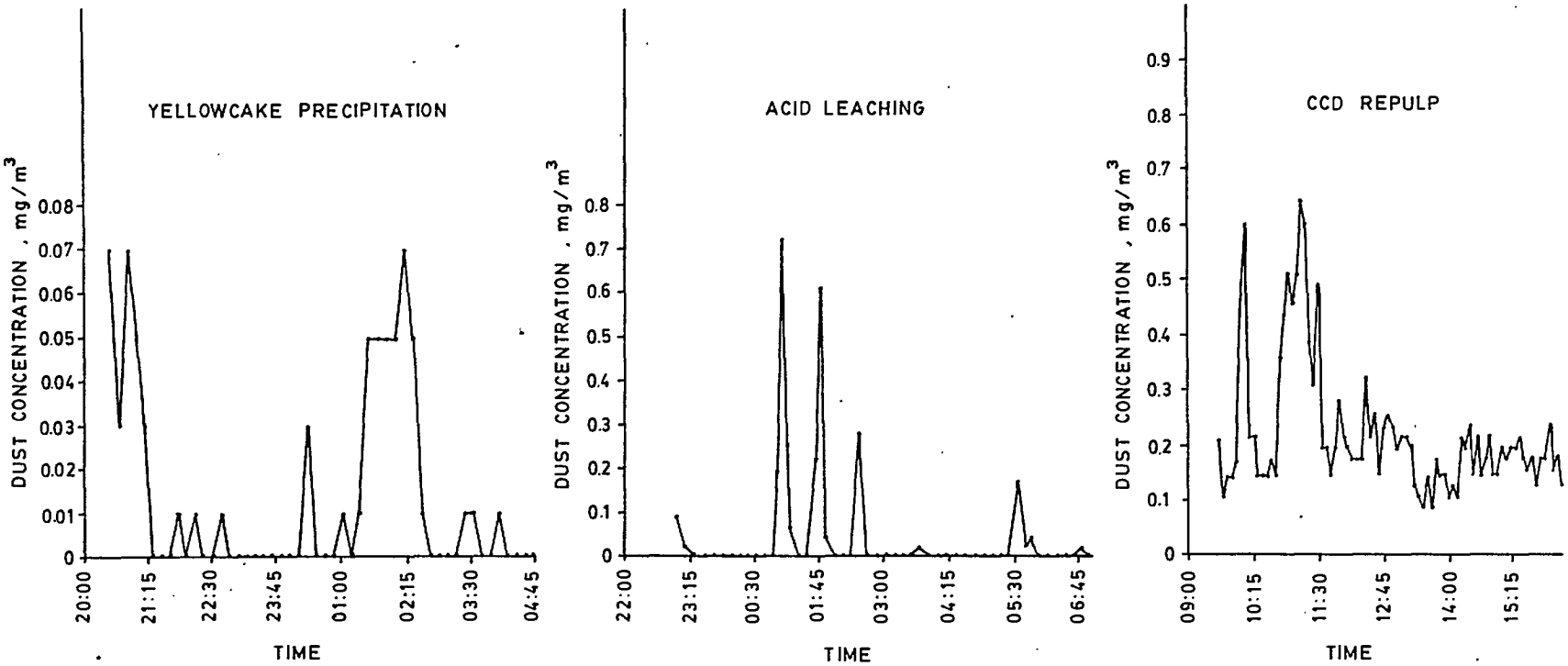

Fig. 16 - Dust concentration for several physico-chemical operations.